RSC Advances

ROYAL SOCIETY OF CHEMISTRY

www.rsc.org/advances

Heterostructured g-C_3N_4/Ag-TiO_2 composites with efficient photocatalytic performance under visible-light irradiation

Mengqiao Zang,[b] Lei Shi,[b] Lin Liang,[c] Defeng Li,[b] Jianmin Sun*[ab]

[a] State Key Laboratory of Urban Water Resource and Environment, Harbin Institute of Technology, Harbin 150080, China

[b] The Academy of Fundamental and Interdisciplinary Science, Harbin Institute of Technology, Harbin 150080, China

[c] School of Life Science and Technology, Harbin Institute of Technology, Harbin 150080, China

Abstract: g-C_3N_4/Ag-TiO_2 composites with close interfacial contact among Ag, TiO_2 and g-C_3N_4 were facilely fabricated and thoroughly characterized. As the deposited Ag nanoparticles played the important roles as an electron-conduction bridge and surface plasmon resonance effect, Ag modification feasibly improved the separation efficiency for photoinduced electron-hole pairs and enhanced visible-light response. Furthermore, due to the further enhanced separation for photogenerated charges resulted from the existed build-in electric field of heterojunction and the superposed light response from hybridization of TiO_2 and g-C_3N_4, g-C_3N_4/Ag-TiO_2 composites exhibited remarkably improved photocatalytic activities for degrading Rhodamine B dye compared with pristine TiO_2 and g-C_3N_4 and single-component modified photocatalysts. Additionally, g-C_3N_4/Ag-TiO_2 catalyst retained excellent stability even after five recycles.

Keywords: Photocatalysis; Ag; TiO_2; g-C_3N_4; Visible light

Corresponding author. Tel.:+86 451 86403715; fax: +86 451 86403715.

E-mail address: sunjm@hit.edu.cn (J.M. Sun).

1. Introduction

Nowadays, the photocatalysis technique is considered to be one of the most promising techniques for solving the global energy crisis and environmental pollution. TiO_2 becomes the most extensively researched photocatalyst due to its low cost, nontoxicity and long-term stability. Fujishima and Honda first reported the decomposition of water on illuminated TiO_2 electrodes in 1972.[1] However, its large band gap energy of 3.2 eV and the high recombination rate of electron-hole pairs seriously restricted the practical application of TiO_2.[2-7] Therefore, it is of great significance to develop novel visible-light-responsive photocatalysts by enhancing light harvesting and reducing the recombination rates of the photoinduced electron-hole pairs.

Recently, graphitic carbon nitride (g-C_3N_4) as a metal-free semiconductor with suitable band gap to absorb the visible light and the unique properties has attracted attentions in photocatalytic performance for H_2 generationor organic pollutant degradation.[8-14] It has been reported that the photocatalytic activity of the semiconductor could be improved by g-C_3N_4 modification. Ge *et al*.[9] developed novel visible-light induced g-C_3N_4/Bi_2WO_6 composite photocatalyst, which exhibited significantly enhanced photocatalytic performance in degrading methyl orange. Pan *et al*.[10] fabricated core/shell structured C_3N_4/$BiPO_4$ photocatalyst via a facile ultrasonic dispersion method. The optimum photocatalytic activity for degradation of methylene blue (MB) over C_3N_4/$BiPO_4$ was almost 4.5 times as high as that of reference catalyst P25 and 2.5 times of $BiPO_4$. Sridharan *et al*.[11] prepared g-C_3N_4/TiO_2 composite through a thermal transformation methodology and investigated the photocatalytic activity of MB and Cr (VI) ions under visible light. Moreover, it was well recognized that Ag modification was a feasible method to improve the separation efficiency for photoinduced electron-hole pairs due to the excellent conductivity and strong electron trapping ability.[17] Besides, the surface plasmon resonance (SPR) effect of Ag enhanced visible-light response of semiconductor, contributing to the utilization of solar energy.[18] Therefore, TiO_2 modified by Ag and g-C_3N_4 would combine peculiar characteristics of the three-component composites and seemed to be an ideal

photocatalyst compared with single-component modified TiO_2.

In this contribution, the heterostructured g-C_3N_4/Ag-TiO_2 composites were facilely fabricated via physical mixing followed by calcination method. Close interfacial contact among Ag, TiO_2 and g-C_3N_4 made the g-C_3N_4/Ag-TiO_2 composites display the reduced recombination efficiency for photoinduced electron-hole pairs and enhanced visible-light absorbance. The synergistic positive effects contributed to g-C_3N_4/Ag-TiO_2 composites better activity for degrading the model pollutant of Rhodamine B (RhB) under visible-light irradiation than the bare g-C_3N_4 and TiO_2 and single-component modified photocatalysts. In addition, g-C_3N_4/Ag-TiO_2 catalyst retained excellent stability even after five recycles. Besides, the tentative photodegradation process over g-C_3N_4/Ag-TiO_2 composites was proposed based on the experimental results.

2. Experimental

2.1 The preparation of the photocatalysts

g-C_3N_4 was prepared by heating 5 g melamine at 600 °C for 2 h with the heating rate of 2 °C/min in a muffle furnace.[19] After being naturally cooled to room temperature, faint yellow g-C_3N_4 was obtained.

Ag-loaded TiO_2 (Ag-TiO_2) was prepared through photodeposition procedure.[20] 0.5 g TiO_2 (P25) was dispersed in 100 mL deionized water and 3 mL 0.05 M $AgNO_3$ solution were added slowly under stirring, then the mixture was irradiated under 300 W Xe-lamp for 3 h with continuous magnetic stirring. After centrifugation, the sample was washed with water and dried at 80 °C overnight to obtain 3 wt% Ag-TiO_2. For comparison, Ag loaded g-C_3N_4 (Ag-C_3N_4) was prepared according to the similar photodeposition procedure.

g-C_3N_4/Ag-TiO_2 composites were prepared as follows: g-C_3N_4 and Ag-TiO_2 with different mass ratios were dispersed in 100 mL distilled water to obtain uniform solution by ultrasonic treatment for 3 h, then the mixture was dried at 60 °C for 12 h and heated at 400 °C for 1 h with the heating rate of 2 °C/min. A series of g-C_3N_4/Ag-TiO_2 composites with mass ratios of g-C_3N_4 to Ag-TiO_2 from 1:9 to 9:1 were

synthesized and denoted as g-C_3N_4/Ag-TiO_2-X. For example, g-C_3N_4/Ag-TiO_2-10 represents the mass percentage of g-C_3N_4 in the g-C_3N_4/Ag-TiO_2 composites is 10%.

2.2 Characterization

X-ray diffraction (XRD) measurements were carried out on Bruker D8 Advance X-ray powder diffractometer with Cu Kα radiation (40 kV, 30 mA) for phase identification. X-ray photoelectron spectroscopy (XPS) measurements were recorded on Phi Quantera spectrometer with Al Kα radiation (hv=1486.6 eV). Fourier transform infrared spectroscopy (FT-IR) was recorded in transmission mode from 4000 to 400 cm^{-1} on Perkin Elmer 100 FTIR spectrometer using KBr discs. The morphology and chemical compositions of the composites were examined by transmission electron microscopy (TEM, Tecnai G2 Spirit) and scanning electron microscopy (SEM, HITACHI SU8000) with energy dispersive X-ray spectroscopy (EDS) mapping. Nitrogen adsorption-desorption isotherms were measured at -196 °C on ASAP 2020 volumetric analyzer. UV-vis diffuse reflectance spectra (DRS) were measured on Perkin Elmer Lambda 750 UV-vis spectrometer. Photoluminescence spectra (PL) were obtained using Perkin Elmer LS55 at room temperature with the excitation wavelength of 325 nm.

2.3 Evaluation of photocatalytic performance

The photocatalytic performance of the as-prepared g-C_3N_4/Ag-TiO_2 composites were examined by degrading RhB dye. The visible light was provided by 300 W Xe-lamp with a 400 nm cut-off filter. 50 mg photocatalyst was added into 50 mL 5 $mg{\cdot}L^{-1}$ RhB aqueous solution, prior to the light irradiation, the dispersion was kept in dark for 30 min to reach the adsorption-desorption equilibrium under magnetic stirring. The distance between the surface of the suspension and the light source was about 20 cm. Solutions were collected every 5 min irradiationand centrifuged to remove the catalyst then analyzed on UV-vis spectrometer. For comparison, the reactions were carried out in the presence of g-C_3N_4, P25, Ag-TiO_2 and Ag-C_3N_4. The degradation efficiency was calculated using C/C_0, wherein C was the concentration of the remaining dye

solution at each irradiated time, and C_0 was the initial concentration.

3. Results and discussion

3.1 Structure, morphology and spectra characterizations of g-C_3N_4/Ag-TiO_2 composites

The XRD patterns of g-C_3N_4/Ag-TiO_2 composites were shown in Fig 1. The peaks at 25.3°, 37.8°, 47.9°, 53.8°, 55.1°, 62.7°, 68.7°, 70.3° and 75.0° were attributed to (101), (004), (200), (105), (211), (204), (116), (220) and (215) crystal planes of anatase TiO_2.[21] For g-C_3N_4, the peaks at 27.4° and 13.1° were corresponded to (002) and (100) planes of hexagonal g-C_3N_4 (JCPDS card no. 87-1526), and respectively attributed to the graphite-like stacking and in-plane structural repeating motifs of the conjugated aromatic units.[22] It was obvious that both TiO_2 and g-C_3N_4 were observed in the composites, and the peak intensities at 27.4° became stronger with the increasing contents of g-C_3N_4in the composites. Nevertheless, there appeared no peaks ascribed to Ag, which might be ascribed to its lower content or its high dispersity.[23]

（Fig. 1）

Fig 2 showed the XPS spectra of g-C_3N_4/Ag-TiO_2-50 composites. In C 1s spectrum, three deconvoluted peaks appeared at 284.3, 286.0 and 287.8 eV. The peak at 284.3 eV was assigned to C-C and the adventitious carbon, and the peaks at 286.0 and 287.8 eV were ascribed to C-N-C and the C-$(N)_3$ coming from g-C_3N_4.[24] For the N 1s spectrum, three peaks at 397.9, 398.6 and 399.9 eV were separately belonged to sp^2-bonded N to two carbon atoms (C=N-C), tertiary nitrogen (N-$(C)_3$) and amino functional group with a hydrogen atom (N-H).[25,26] O 1s spectrum was fitted into two peaks of Ti-O bond at 529.4 eV and O-H bond at 530.4 eV.[27,28] Ti 2p spectrum showed two symmetric peaks at 458.2 and 463.9 eV, which ascribed to electron binding energies of Ti $2p_{3/2}$ and $2p_{1/2}$.[27,28] As shown in Fig 2E, the peaks at 367.0 and 373.1 eV were attributed to Ag $3d_{3/2}$ and Ag $3d_{5/2}$,[29,30] which confirmed the existence of Ag in the composites.

(Fig. 2)

Fig 3 depicted the FT-IR spectra of the bare g-C_3N_4, TiO_2, and g-C_3N_4/Ag-TiO_2-50 composites. For the bare g-C_3N_4, there were three main absorption regions to be observed clearly. The peaks at 1640, 1247, 1325 and 1408 cm^{-1} were associated with the stretching vibrations of CN heterocycles.[15,31] The peak at 808 cm^{-1} was attributed to the characteristic breathing modes of triazine units.[15] The broad peak at 3150-3500 cm^{-1} was assigned to the stretching vibration modes of terminal N-H and O-H.[32] In the case of TiO_2, a broad absorption band at 500-700 cm^{-1} was regarded as the characteristic peak of TiO_2.[33] The FT-IR spectra of the g-C_3N_4/Ag-TiO_2-50 composites represented the characteristic peaks of both g-C_3N_4 and TiO_2, indicative of their coexistence in the composites.

(Fig. 3)

Fig 4 showed the TEM images of the bare g-C_3N_4, TiO_2 and g-C_3N_4/Ag-TiO_2-50 composites. The pristine g-C_3N_4 displayed aggregation of 2D lamellar structure, and TiO_2 presented as agglomerates of small spherical-like particles. For g-C_3N_4/Ag-TiO_2-50 composites in Fig 4C, it was observed that TiO_2 and Ag nanoparticles highly dispersed on the g-C_3N_4 surface. Additionally, HRTEM image of g-C_3N_4/Ag-TiO_2-50 composites (Fig 4D) clearly revealed the interface between g-C_3N_4 and Ag-TiO_2, and an discerned interplanar spacing of 0.35 nm conforms to the (101) crystal plane of TiO_2 while 0.23 nm matches with the (111) plane of Ag.[34] Therefore, the close interfacial contact could facilitate the photogenerated electron transfers from g-C_3N_4 to Ag or TiO_2 nanoparticles. Hence, it was reasonable that an improved photocatalytic activity was expected for the as-prepared g-C_3N_4/Ag-TiO_2 composites.

(Fig. 4)

The EDS elemental mappings further indicated that g-C_3N_4/Ag-TiO_2-50 composites were composed of C, N, Ti, O and Ag elements, which were evenly dispersed. Thus the composites coupled with g-C_3N_4, Ag and TiO_2 were successfully fabricated.

(Fig. 5)

Nitrogen adsorption-desorption analysis in Fig. 6 was used to determine BET surface areas of the catalysts, the surface areas of the as-prepared samples were 35.77

m^2 g^{-1}, 26.45 m^2 g^{-1}, 27.19 m^2 g^{-1}, 18.07 m^2 g^{-1}, 10.97 m^2 g^{-1} and 4.99 m^2 g^{-1} for g-C_3N_4/Ag-TiO_2-10, g-C_3N_4/Ag-TiO_2-30, g-C_3N_4/Ag-TiO_2-50, g-C_3N_4/Ag-TiO_2-70, g-C_3N_4/Ag-TiO_2-90 and bare g-C_3N_4.

(Fig 6)

The absorbance properties of the as-prepared samples were measured using UV-vis DRS in Fig 7. A sharp basal absorption edge for TiO_2 appeared at 393 nm, corresponding to the electron transition of bandgap at 3.2 eV. Ag-TiO_2 showed obvious light absorption in the visible-light region, which was ascribed to the SPR effect of the loaded Ag nanoparticles.[35] The main absorption edge of g-C_3N_4 occurred at 473 nm due to its narrowed bandgap. Noticeably, g-C_3N_4/Ag-TiO_2-50 composites displayed significantly enhanced visible-light absorption due to the loaded Ag and the superposed absorption from g-C_3N_4 and TiO_2. The bandgap energies (E_g) of bare TiO_2 particle, g-C_3N_4, Ag-TiO_2 and g-C_3N_4/(Ag-TiO_2)-50 composites were calculated to be 3.16 eV (TiO_2), 2.62 eV (g-C_3N_4), 2.95 eV (Ag-TiO_2) and 2.57 eV (g-C_3N_4/Ag-TiO_2) according to $E_g=1240/\lambda_g$ euqation.[33] And based on the empirical equations of $E^0_{VB}=\chi-E^C-1/2E_g$ and $E_{CB}=E_{VB}-E_g$,[36] the potentials of VB and CB of g-C_3N_4 were calculated at -1.105 eV and 1.515 eV, and those of TiO_2 were -0.295 eV and 2.865 eV. After the light illuminated, the photoinduced electrons were generated on g-C_3N_4 and easily transferred from CB of g-C_3N_4 to the CB of TiO_2 via the interface. Namely, the CB of TiO_2 could act as a sink for photo generated electrons, benefitting the separation of electrons and holes.

(Fig. 7)

3.2 Photocatalytic activity for degrading RhB

The photocatalytic activity of degrading RhB was shown in Fig 8A, when g-C_3N_4 and P25 were added, RhB concentration gradually decreased and the degradation efficiencies were 86% and 40% within 30 min. By contrast, the photocatalytic activities over Ag-TiO_2 and Ag-C_3N_4 were enhanced by Ag modifications. With the co-modifications of Ag and g-C_3N_4, the photocatalytic activities of g-C_3N_4/Ag-TiO_2 were remarkably improved. The activities were in the

order of g-C_3N_4/Ag-TiO_2-10<g-C_3N_4/Ag-TiO_2-70<g-C_3N_4/Ag-TiO_2-90<g-C_3N_4/Ag-TiO_2-30<g-C_3N_4/Ag-TiO_2-50. In the case of g-C_3N_4/Ag-TiO_2-10 composites, photocatalytic activity was low resulted from the reduced visible-light harvesting due to the low content of g-C_3N_4. With more contents of g-C_3N_4 at mass ratios of g-C_3N_4/Ag-TiO_2 7:1 and 9:1, although the absorptions to visible light were enhanced, the high recombination rates of photoinduced charges because of low contents of active separation centers acted by TiO_2 and Ag led to the decreased activities. Thus the optimum catalytic performance was obtained in the g-C_3N_4/Ag-TiO_2-50 composites, after 30 min visible-light irradiation, the removal efficiency of RhB was improved to 96%.To have a better understanding of the reaction kinetics of RhB degradation catalyzed by various catalysts, the relationships between $\ln(C_0/C)$ and irradiation time were depicted in Fig 8B. The linear relationships suggested that the photocatalytic degradation curves in all cases fit well with pseudo-first-order kinetics. The kinetic constants were 0.0983 min^{-1} for g-C_3N_4/Ag-TiO_2-50, 0.0391 min^{-1} over g-C_3N_4/TiO_2 (mass ratio 1:1), 0.0156 min^{-1} over TiO_2, 0.0603 min^{-1} over g-C_3N_4, 0.0445 min^{-1} over Ag-TiO_2, and 0.0653 min^{-1} for Ag-C_3N_4. The g-C_3N_4/Ag-TiO_2-50 composites exhibited the highest rate constant, which was almost 6.30 and 1.63 times higher than pure TiO_2 and pure g-C_3N_4, obviously displaying the positive effects of Ag and g-C_3N_4.

(Fig. 8)

From the viewpoint of practical applications, the stability of photocatalyst is a very important factor. As the representative sample, g-C_3N_4/Ag-TiO_2-50 composites were selected to evaluate the reusability. As shown in Fig 9A, the photocatalytic activity of g-C_3N_4/Ag-TiO_2-50 composites still kept at 90% of fresh catalyst even after five recycles, which suggested that g-C_3N_4/Ag-TiO_2 composites possessed excellent stability. In contrast, the physical mixing of g-C_3N_4 and Ag-TiO_2 without calcination showed poor stability even in the second run (Fig. 9B), attribute to the lost contact interaction between g-C_3N_4 and Ag-TiO_2. In addition, the XRD patterns and FT-IR of g-C_3N_4/Ag-TiO_2-50 composites before and after five photodegradation runs

were investigated and shown in Fig 9C-D. After five recycles, the structure of the spent g-C_3N_4/Ag-TiO_2-50 composites was the same to the fresh catalyst, indicative of the structure stability during the photoreaction process.

(Fig. 9)

3.3 Possible photodegradation process

Since photoluminescence emission spectrum arises from the recombination of excited electrons and holes, thus, PL technique is useful for disclosing the migration, transfer and recombination processes of the photogenerated electron-hole pairs in the semiconductors. The lower PL intensity is a general indication of the lower recombination of electron-hole pairs. Fig 10 showed the PL spectra of g-C_3N_4, Ag-C_3N_4 and g-C_3N_4/Ag-TiO_2-50 composites with the excitation wavelength of 325 nm. Pristine g-C_3N_4 exhibited much stronger intensity than g-C_3N_4/Ag-TiO_2-50 composites. For g-C_3N_4/Ag-TiO_2-50 composites, the lower intensity meant that the loaded Ag and existed heterojunction facilitated charge transfers among Ag, TiO_2 and g-C_3N_4, leading to the decreased recombination probability of the electrons-holes and the improved photocatalytic activity.

(Fig. 10)

In order to investigate the main reactive species for the photodegradation of the RhB, the addition effects of radical scavengers were examined to discuss the reaction mechanism (Fig. 11). Here, methanol was used to quench ·OH in the solution,[37] EDTA was h^+ scavenger,[38] p-benzoquinone (p-BQ) was $\cdot O_2^-$ quencher,[39] and dimethyl sulfoxide (DMSO) was e^- scavenger.[40] The additions of methanol, EDTA and DMSO led to the remarkable decreases in degradation activities, which implied that ·OH, h^+ and e^- were the active reactive species. The addition of p-BQ made the degradation of RhB almost inhibit, suggesting that $\cdot O_2^-$ was the main reactive species, which was consistent with the previous report.[41]

(Fig. 11)

Based on the above results, a possible photodegradation mechanism over g-

C_3N_4/Ag-TiO_2 composites were proposed in Fig 12. During the photocatalytic oxidation process, g-C_3N_4 first was excited to form photogenerated electron-hole pairs under visible-light irradiation. The CB and VB edge potentials of g-C_3N_4 were at -1.105 and +1.515 eV, more negative than those of TiO_2 at -0.295 and +2.865 eV. Subsequently, the photogenerated electrons transferred from CB of g-C_3N_4 to TiO_2 or trapped by Ag nanoparticles. These electrons further reacted with O_2 adsorbed on the catalyst surface to generate $\cdot O^-_2$, and $\cdot O^-_2$ radicals combined with H_2O to further transformed to ·OH. At the same time, h^+ in the VB of g-C_3N_4 was less positive than the standard redox potential of ·OH/H_2O (2.68 eV vs. SHE),[42] indicating that the photogenerated holes on the g-C_3N_4 could not oxidize H_2O into ·OH, but directly involved into the degradation of pollutant. And h^+ in the VB of TiO_2 is more positive than the standard redox potential of ·OH/H_2O, so they could combine with H_2O to produce active ·OH. These reactive radical species of $\cdot O^-_2$, ·OH, h^+ and e^- were so reactive that they could efficiently react with the organic pollutant to generate the degradation products. In the photocatalytic reaction process, the recombination rates of the electrons and holes were efficiently prevented and the absorption to the visible light was significantly enhanced, thus resulting in the enhanced photocatalytic activity over g-C_3N_4/Ag-TiO_2 composites.

(Fig. 12)

4. Conclusion

In summary, g-C_3N_4/Ag-TiO_2photocatalyst was facilely synthesized and exhibited enhanced visible-light-driven activity for degrading RhB. And g-C_3N_4/Ag-TiO_2 with mass ratio ofg-$C_3N_4$to Ag-TiO_2 at 1:1 showed the optimal photodegradation efficiency and excellent stability. The interfacial contact existed in the g-C_3N_4/Ag-TiO_2 composites contribute to retarding the charge recombinations, moreover, the deposited Ag nanoparticles played an important role as electron reservoir for the efficient separation of electrons-holes. Besides, the enhanced absorption to the visible light coming from the Ag SPR effect and superpose absorption from g-C_3N_4coupled with TiO_2 also assisted the improvement of catalytic activity. Therefore, g-C_3N_4/Ag-

TiO_2 composites may be potential photocatalyst candidate applied in environmental pollutants removal.

Acknowledgement

We sincerely acknowledge the financial supports from National Natural Science Foundation of China (21373069), Science Foundation of Harbin City (NJ20140037), State Key Lab of Urban Water Resource and Environment of Harbin Institute of Technology (HIT2015DX08) and the Fundamental Research Funds for the Central Universities (HIT. IBRSEM. 201327).

References

1. A. Fujishima and K. Honda. *Nature*, 1972, **238,** 37-38.
2. J. Li, F. Sun, K. Gu, T. Wu, W. Zhai, W. Li and S. Huang,*Appl. Catal. A: Gen.*, 2011, **406**, 51-58.
3. F. Yang, N. Yan, S. Huang, Q. Sun, L. Zhang and Y. Yu, *J. Phys. Chem. C*, 2012, **116**, 9078-9084.
4. M.R. Hoffman, S.T. Martin and W. Choi, *Chem. Rev.*, 1995, **95**, 69-96.
5. A.L. Linsebigler, G. Lu and J.T. Yates, *Chem. Rev.*, 1995, **95**, 735-758.
6. R.L. Narayana, M. Matheswaran, A.A. Aziz and P. Saravanan, *Desalination*, 2011, **269**, 249-253.
7. X. Pan, Y. Zhao, S. Liu, C.L. Korzeniewski, S. Wang and Z. Fan, *Appl. Mater. Interfaces*, 2012, **4**, 3944-3950.
8. X.C. Wang, K. Maeda, A. Thomas, K. Takanabe, G. Xin, J.M. Carlsson, K. Domen and M. Antonietti, *Nat. Mater.*, 2009, **8**, 76-80.
9. L. Ge, C.G. Han and J. Liu, *Appl. Catal. B: Environ.*, 2011, **108**, 100-107.
10. C. Pan, J. Xu, Y.J. Wang, D. Li and Y.F. Zhu, *Adv. Funct. Mater.*, 2012, **22**, 1518-1524.
11. K. Sridharan, E. Jang and T.J. Park, *Appl. Catal. B: Environ.*, 2013, **142**, 718-728.
12. L. Shi, L. Liang, J. Ma, F.X. Wang and J.M. Sun, *Catal. Sci. Technol.*, 2014, **4**, 758-765.

13. L. Shi, L. Liang, J. Ma, F.X. Wang and J.M. Sun, *Dalton Trans.*, 2014, **43**, 7236-7244.
14. L. Shi, L. Liang, F.X. Wang, M.S. Liu, S.F. Zhong and J.M. Sun, *Catal. Commun.*, 2015, **59**, 131-135.
15. Y. J. Wang, R. Shi, J. Lin and Y.F. Zhu, *Energy Environ. Sci.*, 2011, **4**, 2922-2929.
16. J.X. Sun, Y.P. Yuan, L.G. Qiu, X. Jiang, A.J. Xie, Y.H. Shen and J.F. Zhu, *Dalton Trans.*, 2012, **41**, 6756-6763.
17. S. Sakthivel, M.V. Shankar, M. Palanichamy, B. Arabindoo, D.W. Bahnemann and V. Murugesan, *Water Res.*, 2004, **38**, 3001-3008.
18. A. Atrei, A.M. Ferrari, D. Szieberth, B. Cortigiani and G. Rovida, *Phys. Chem. Chem. Phys.*, 2010, **12**, 11587-11595.
19. Y. Wang, X.C. Wang and M. Antonietti, *Angew. Chem. Int. Ed.*, 2012, **51**, 68-89.
20. Q. Xiang, J. Yu and M. Jaroniec, *J. Phys. Chem. C*, 2011, **115**, 7355-7363.
21. N. Boonprakob, N. Wetchakun, S. Phanichphant, J. Chen and B. Inceesungvorn, *Adv. Mater. Res.*, 2013, **622-623**, 883-888.
22. M. Groenewolt and M. Antonietti, *Adv. Mater.*, 2005, **17**, 1789-1792.
23. X.Y. Pan and Y. Xu, *J. Phys. Chem. C*, 2013, **117**, 17996-18005
24. J. A.Singh, S. H. Overbury, N. J. Dudney, M.J. Li, and G.M. Veith, *ACS Catal.*, 2012, **2**, 1138-1146.
25. J.H. Liu, T.K. Zhang, Z.C. Wang, G. Dawson and W. Chen, *J. Mater. Chem.*, 2011, **21**, 14398-14401.
26. F. Dong, L.W. Wu, Y.J. Sun, M. Fu, Z.B. Wu and S.C. Lee, *J. Mater. Chem.*, 2011, **221**, 15171-15174.
27. B. Chai, T.Y. Peng, P. Zeng and J. Mao, *J. Mater. Chem.*, 2011, **21**, 14587-14593.
28. G.M. An, W.H. Ma, Z. Y. Sun and J. C. Zhao, *Carbon*, 2007, **45**, 1795-1801.
29. L.Q. Ye, J.Y. Liu, C.Q. Gong, L.H. Tian, T.Y. Peng and L. Zan, *ACS Catal.*, 2012, **2**, 1677-1683.
30. Z.H. Chen, W.L. Wang, Z.G. Zhang and X.M. Fang, *J. Phys. Chem. C*, 2013, **117**, 19346-19352.
31. S.C. Yan, S.B. Lv, Z.S. Li and Z.G. Zou, *Dalton Trans.*, 2010, **39**, 1488-1491.

32. Y. Zhao, Z. Liu, W. Chu, L. Song, Z. Zhang, D. Yu, Y. Tian, S. Xie and L. Sun, *Adv. Mater.*, 2008, **20**, 1777-1781.
33. B. Chai, T. Peng, J. Mao, K. Li and L. Zan, *Phys. Chem. Chem. Phys.*, 2012, **14**,16745-16752.
34. M.B. Suwarnkar, R.S. Dhabbe, A.N.Kadam, K.M. Garadkarn, *Ceram. Int*., 2014, **40**, 5489-5496.
35. J.G. Yu, L.F. Qi and M. Jaroniec, *J. Phys. Chem. C*, 2014, **114**, 13118-13125.
36. Y. Xu and M.A.A. Schoonen, *Am. Mineral.*, 2000, **85**, 543-556.
37. R. Dong, B. Tian, J. Zhang, T. Wang, Q. Tao, S. Bao, F. Yang and C. Zeng, *Catal. Commun.*, 2013, **38**, 16-20.
38. D. Wang, L. Shi, Q. Luo, X. Li and J. An, *J. Mater. Sci.*, 2012, **47**, 2136-2145.
39. C. Hu, T.W. Peng, X.X. Hu, Y.L. Nie, X.F. Zhou, J.H .Qu and H. He, *J. Am. Chem. Soc.*, 2010, **132**, 857-862.
40. D. Wang, Y. Duan, Q. Luo, X. Li, J. An, L. Bao and L. Shi, *J. Mater. Chem. A*, 2012, **22**, 4847-4854.
41. L. Shi, L. Liang, J. Ma, Y.N. Meng, S.F. Zhong, F.X. Wang and J.M. Sun, *Ceram. Int.*, 2014, **40**, 3495-3502.
42. S. Zhao, S. Chen, H. Yu and X. Quan, *Sep. Purif. Technol.*, 2012, **99**, 50-54.

Figure Captions

Fig. 1 XRD patterns of (a) g-C_3N_4, (b) g-C_3N_4/Ag-TiO_2-90, (c) g-C_3N_4/Ag-TiO_2-70, (d) g-C_3N_4/Ag-TiO_2-50, (e) g-C_3N_4/Ag-TiO_2-30, (f) g-C_3N_4/Ag-TiO_2-10, (g) TiO_2 and (h) Ag-TiO_2.

Fig. 2 XPS spectra of g-C_3N_4/Ag-TiO_2-50, (A) C 1s, (B) N 1s, (C) O 1s, (D) Ti 2p and (E) Ag 3d.

Fig. 3 FT-IR spectra of (a) g-C_3N_4, (b) g-C_3N_4/Ag-TiO_2-50 and (c) TiO_2.

Fig. 4 TEM images of (A) bare g-C_3N_4, (B) TiO_2, (C) g-C_3N_4/Ag-TiO_2-50 composites and (D) HRTEM image of g-C_3N_4/Ag-TiO_2-50 composites.

Fig. 5 SEM image of g-C_3N_4/Ag-TiO_2-50 and corresponding EDS mapping images for rectangle area.

Fig. 6 Nitrogen adsorption-desorption isotherms of (a) g-C_3N_4/Ag-TiO_2-10, (b) g-C_3N_4/Ag-TiO_2-30, (c) g-C_3N_4/Ag-TiO_2-50, (d) g-C_3N_4/Ag-TiO_2-70, (e) g-C_3N_4/Ag-TiO_2-90 and (f) g-C_3N_4.

Fig. 7 UV-vis diffuse reflectance absorption spectra of (a) bare TiO_2, (b) Ag-TiO_2, (c) g-C_3N_4 and (d) g-C_3N_4/Ag-TiO_2-50.

Fig. 8 (A) Photodegradation activities and (B) First-order kinetic plots for the photodegradation of RhB; (s1) g-C_3N_4/Ag-TiO_2-10, (s2) g-C_3N_4/Ag-TiO_2-30, (s3) g-C_3N_4/Ag-TiO_2-50, (s4) g-C_3N_4/Ag-TiO_2-70, (s5) g-C_3N_4/Ag-TiO_2-90, (a) P25, (b) g-C_3N_4/TiO_2, (c) Ag-TiO_2, (d) g-C_3N_4 and (e) Ag-C_3N_4.

Fig. 9 Circulating runs in the photodegradation of RhB (A) over g-C_3N_4/Ag-TiO_2-50 composites, (B) over physical mixture of g-C_3N_4 with Ag-TiO_2 without calcination, (C) XRD and (D) FT-IR patterns of g-C_3N_4/Ag-TiO_2-50 composites before and after reuses for the photodegradation of RhB.

Fig. 10 PL spectra of g-C_3N_4, Ag-C_3N_4 and g-C_3N_4/Ag-TiO_2-50 composites.

Fig. 11 Effects of adding different radical scavengers on the degradation of RhB over g-C_3N_4/Ag-TiO_2-50 composites. (a) no scavenger, (b) with 10 mM methanol, (c) with 5 mM DMSO, (d) with 1mM EDTA, and (e) with 1mM p-BQ.

Fig. 12 Possible photodegradation process over g-C_3N_4/Ag-TiO_2 composites under visible-light irradiation.

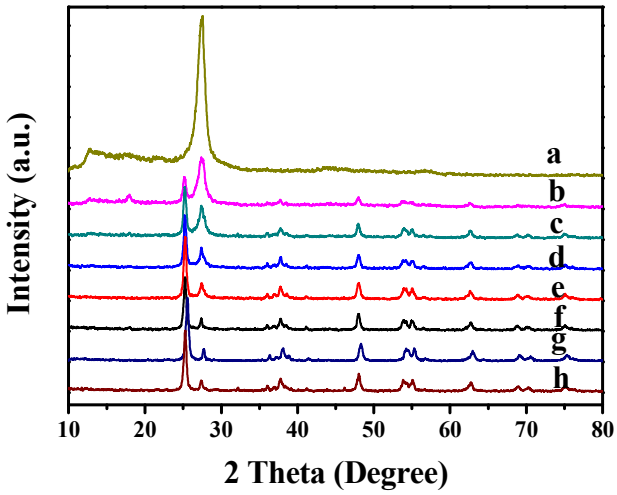

Fig. 1

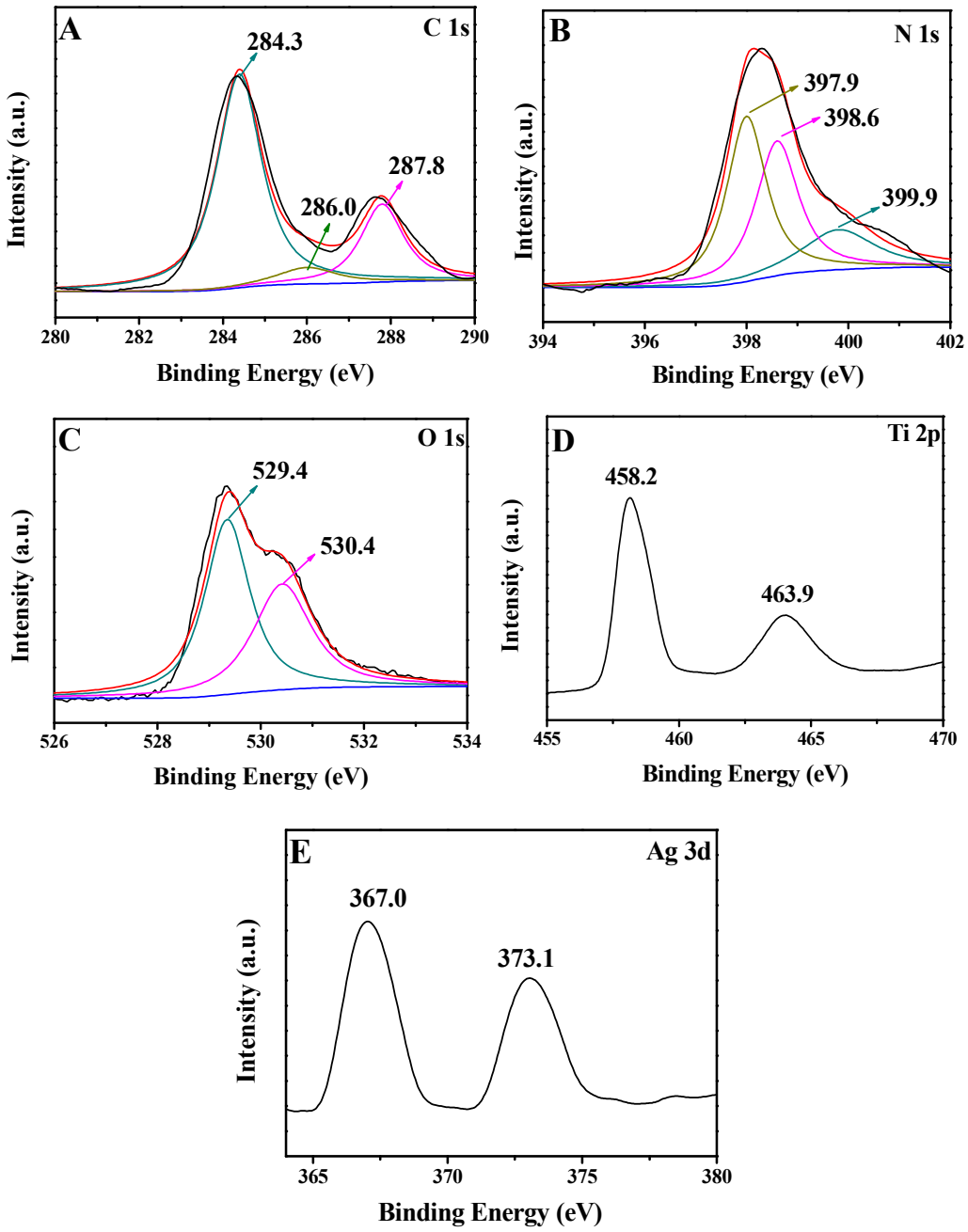

Fig. 2

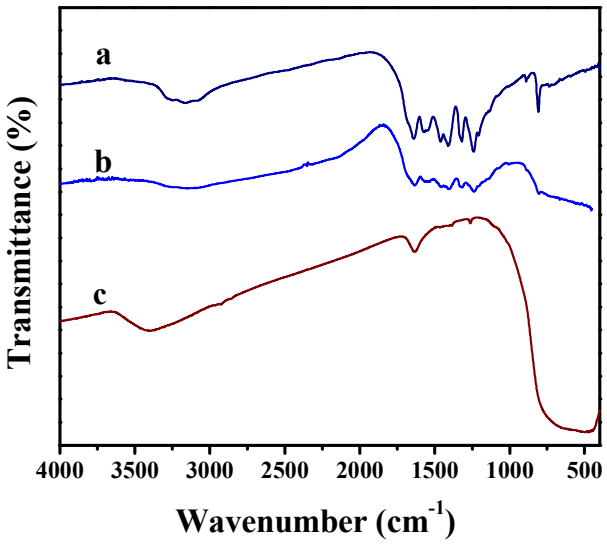

Fig. 3

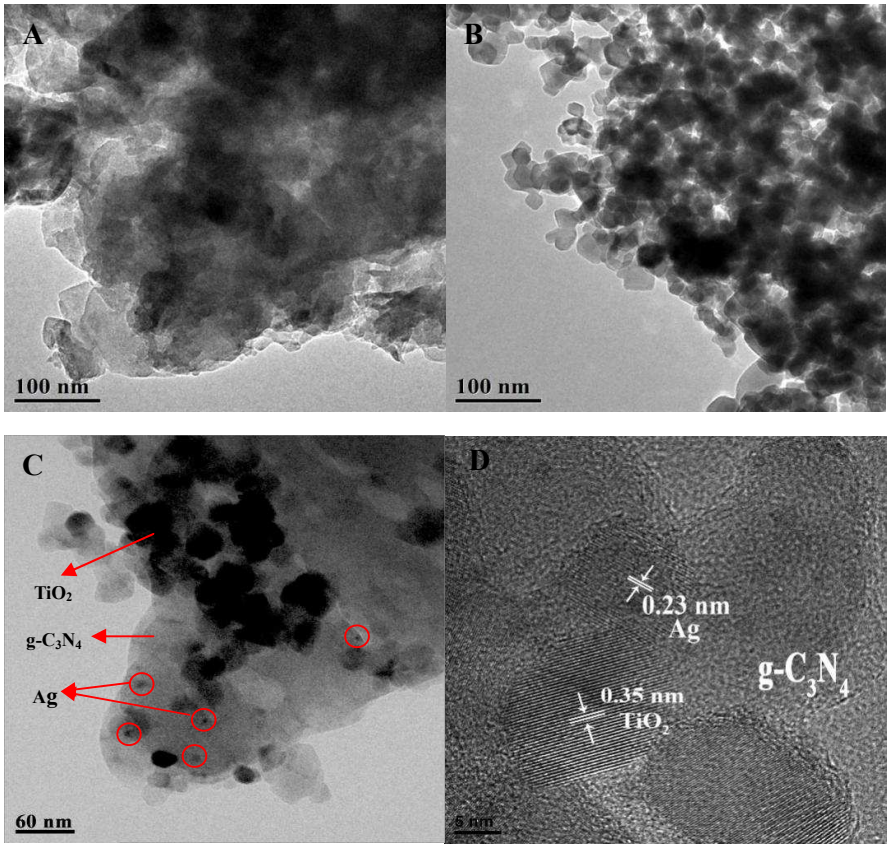

Fig. 4

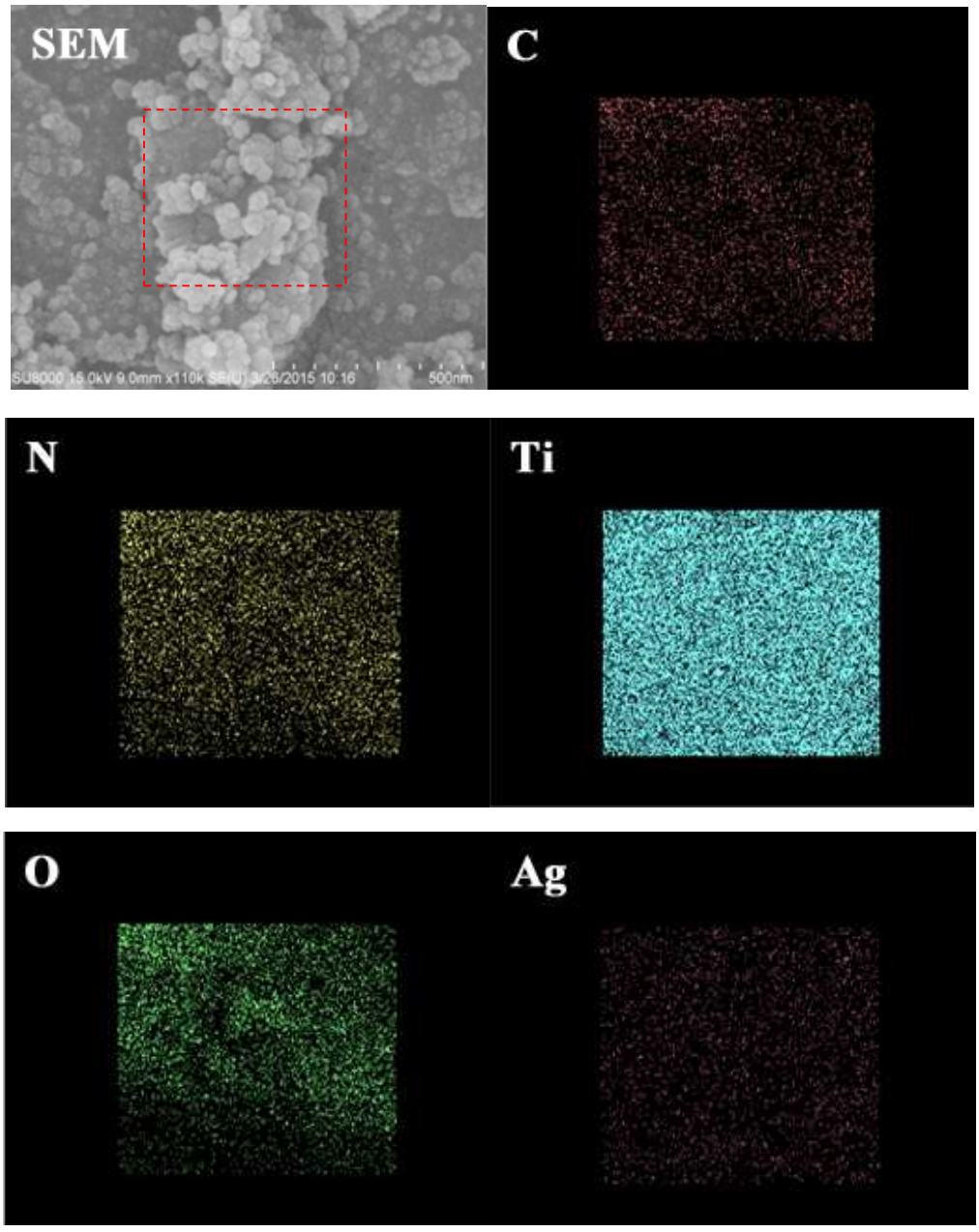

Fig. 5

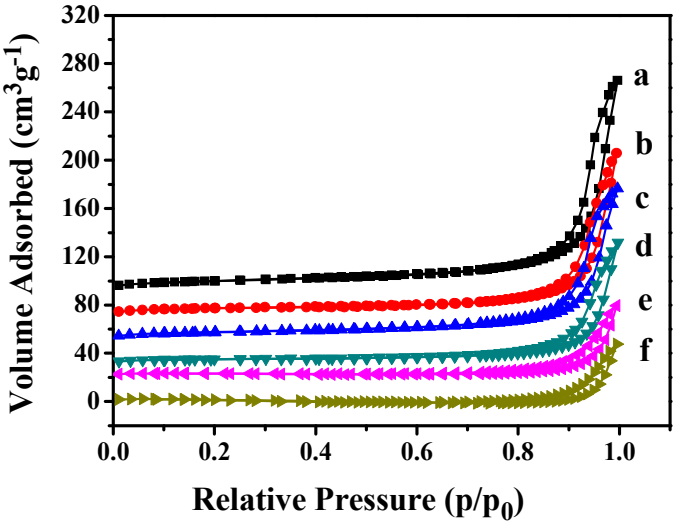

Fig. 6

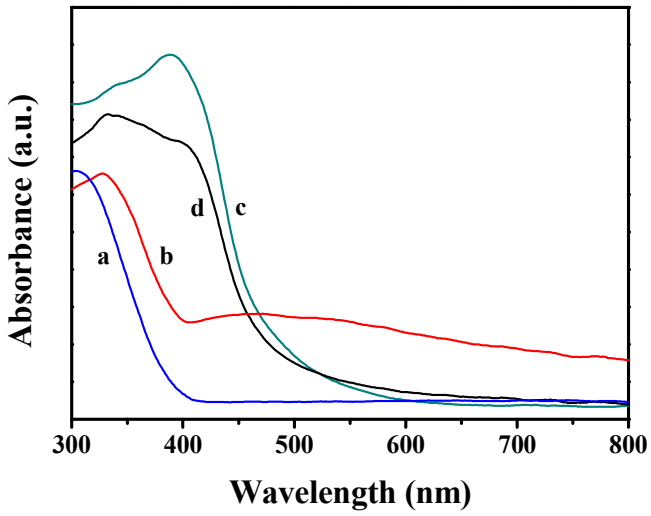

Fig. 7

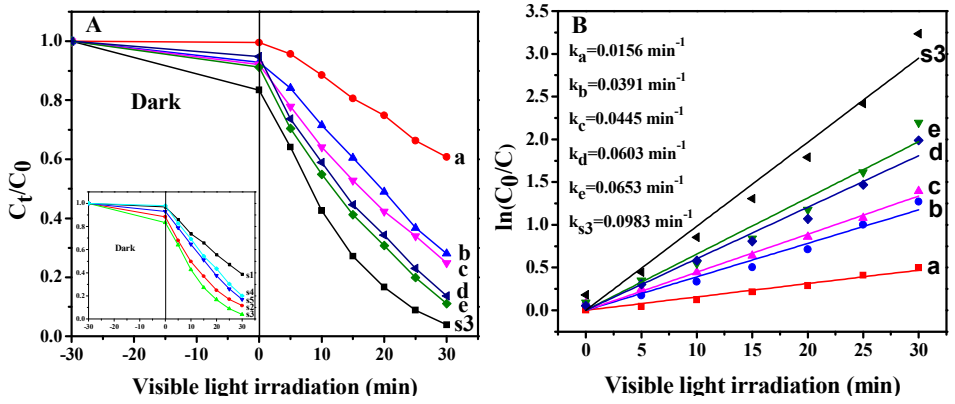

Fig. 8

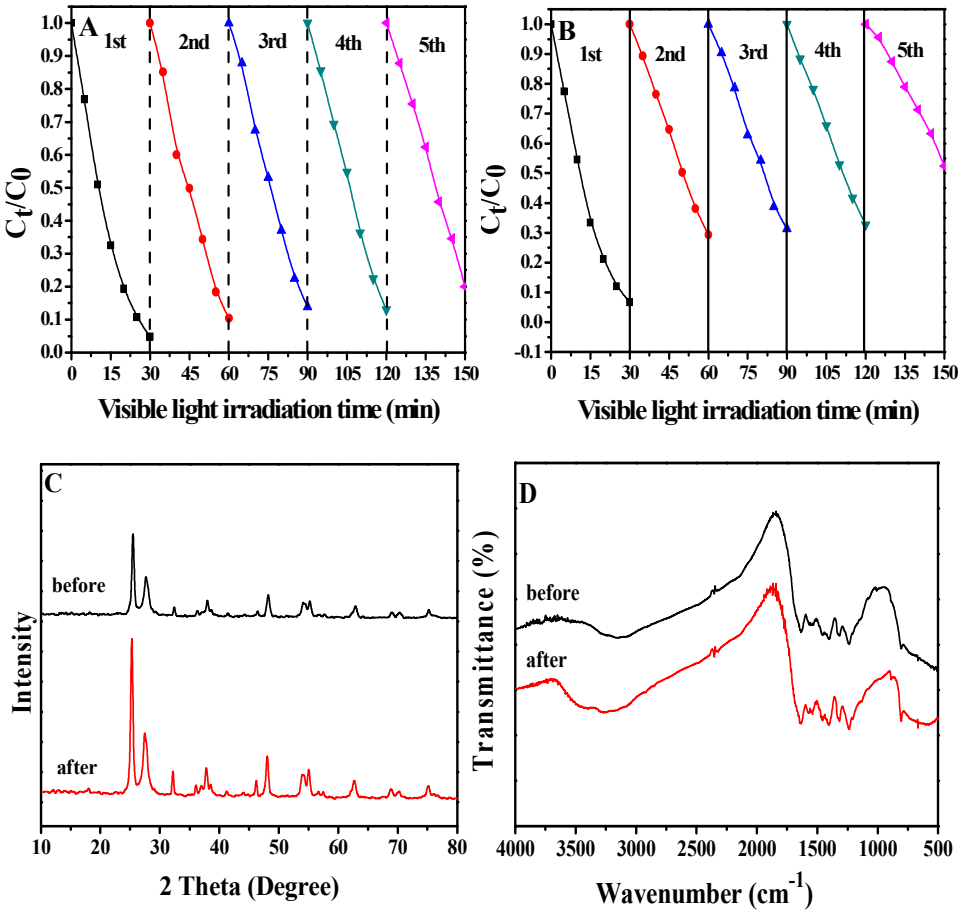

Fig. 9

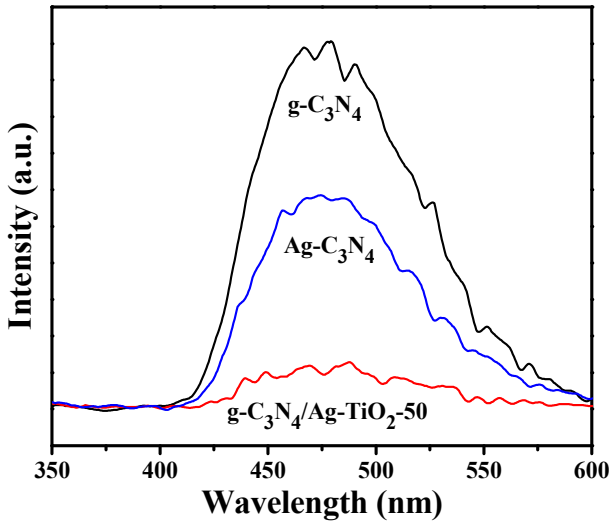

Fig. 10

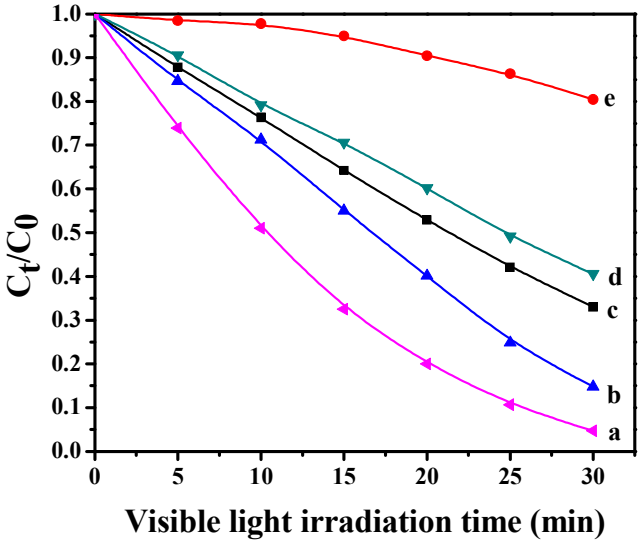

Fig. 11

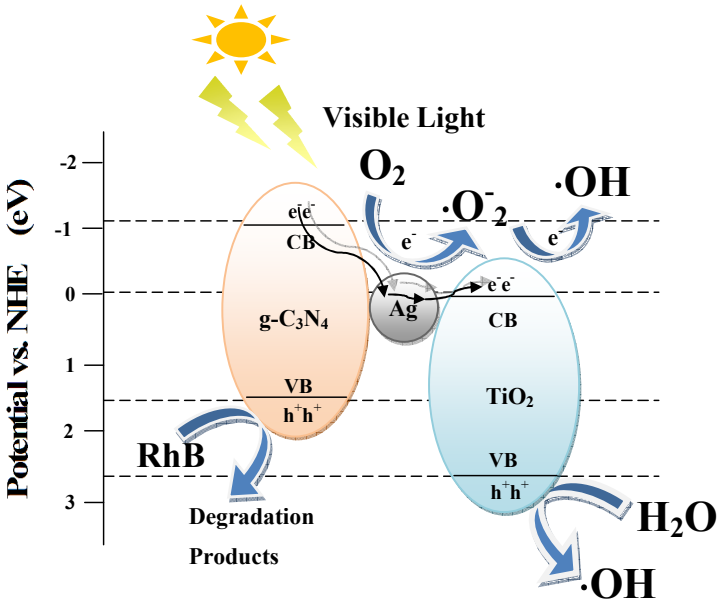

Fig. 12

Graphic Abstract

The heterostructured g-C_3N_4/Ag-TiO_2 composites exhibited highly photocatalytic activity, which was attributed to the synergistic effects of the enhanced absorption of visible light and the efficient separation rates for photogenerated electrons-holes.